

Nanoscale Confinement Effects on the Relaxation Dynamics in Networks of Diglycidyl Ether of Bisphenol-A and Low-Molecular-Weight Poly(ethylene oxide)

Ioannis M. Kalogeras,^{*,†} Andreas Stathopoulos,[†] Aglaia Vassilikou-Dova,[†] and Witold Brostow[‡]

Solid State Physics Section, Department of Physics, University of Athens, Panepistimiopolis, 157 84 Zografos, Greece, and Laboratory of Advanced Polymers & Optimized Materials (LAPOM), Department of Materials Science and Engineering, University of North Texas, P.O. Box 305310, Denton, Texas 76203-5310

Received: October 20, 2006; In Final Form: January 12, 2007

Thermoplastic poly(ethylene oxide) (PEO) ($M_{w(\text{PEO})} \approx 4000$) has been used to prepare thermosetting nanocomposites incorporating diglycidyl ether of bisphenol A (DGEBA) epoxy oligomer. Blends with various PEO/DGEBA weight ratios were cured using stoichiometric portions of 4,4'-diaminodiphenylmethane. The resulting semi-interpenetrating polymer networks were studied by several techniques. Nanoscale confinement effects, thermal (glass transition, melting and crystallization temperatures) and structural features of our materials are similar to those for networks with much higher $M_{w(\text{PEO})}$ and different curing agents; however, the polyether crystallization onset occurs in our case at a lower PEO concentration; shorter PEO chains organize themselves more easily into crystalline domains. Very low estimates of the k parameter of the Gordon–Taylor equation, used to fit the compositional dependences of the dielectric and calorimetric glass transition temperatures, and a strong plasticization of the motion of the glyceryl segments (β -relaxation) in the epoxy resin were observed. These illustrate an intensified weakening in the strength of the intermolecular interactions in the modified networks, as compared to the high strength of the self-association of hydroxyls in the neat resin. The significance of hydrogen-bonding interactions between the components for obtaining structurally homogeneous thermoset-*i*-thermoplastic networks is discussed.

I. Introduction

Polymer networks have been used and investigated for a long time.¹ Desired properties can be achieved more easily in interpenetrating polymer networks (IPNs) in which two (or more) components are held together mainly by topological constraints. Depending on the method of synthesis, the overall composition, the thermodynamical miscibility of the components, the cross-link density and crystallinity, one can obtain IPNs with dispersed-phase domains ranging from a few millimeters to a few tens of nanometers. Extreme cases are either fully mixed or completely phase-separated networks. Frequently observed phase-separated morphologies in thermoset-*i*-polymer networks are believed to arise from a competition among kinetic and thermodynamic factors.^{2–6} Miscibility among components has been discussed in terms of structural similarities and, in particular, in terms of the presence of hydrogen bonding δH ,^{7,8} ion–dipole forces and electron donor–acceptor interactions among the components. Miscibility and specific intermolecular interactions in such systems are much more complicated than in linear polymer blends. Kinetic factors, the curing program, and the topological structures of the system are closely coupled with the thermodynamics of mixing.

Nanocomposites based on thermosets (e.g., epoxy resins, ERs) and linear polyetheric modifiers, such as poly(ethylene oxide) (PEO), are an important group of semi-IPNs presenting a range of micromorphologies. The proton-accepting PEO exhibits

strong interactions and miscibility with polymers containing functional acid groups, such as the poly(hydroxyl ether of bisphenol A) (phenoxy).^{9,10} Diglycidyl ether of bisphenol A (DGEBA)-type epoxies have a structure similar to phenoxy and, thus, are expected to show high compatibility with PEO. Nevertheless, phase-separated morphology has been reported for semi-IPNs formed by thermosetting polymers modified by addition of PEO and several other polyether-type thermoplastics, such as poly(propylene oxide), poly(vinyl ethyl ether), polyacetal(polyoxymethylene), poly(2,6-dimethyl-1,4-phenylene oxide),³ and poly(ether imide).^{4,6} High-molecular-weight PEO has been reported to exhibit miscibility with DGEBA cured with 1,3,5-trihydroxybenzene,⁸ aromatic amines (e.g., 4,4'-methylenebis(2-chloroaniline),¹¹ 4,4'-diaminodiphenylmethane (DDM),¹² 4,4'-diaminodiphenylsulfone (DDS),^{13,14} and 4,4'-methylenebis(3-chloro-2,6-diethylaniline)¹⁵), and aromatic anhydrides (e.g., phthalic anhydride¹⁶ and pyromellitic dianhydride (PMDA)¹⁵). In contrast, immiscibility has been reported for ER-*i*-PEO networks prepared with aliphatic amine curatives, such as diethylene triamine (DETA)¹³ and tetraethylene pentamine.² Experimental observations such as those described above have stimulated extensive research in the field of thermoset-*i*-polymer networks, with particular interest shown for the morphology of the material and the nature and strength of nanoscale interactions. These studies directly address the need to manipulate structural characteristics of the network systems during processing, with the aim to meet the requirements of specific technological applications.

* Corresponding author. E-mail: ikaloger@phys.uoa.gr. Website: <http://www.unt.edu/LAPOM/>.

[†] University of Athens.

[‡] University of North Texas.

In addition to the common search for different component compositions, curatives and curing programs,^{11–16} an interesting, but hardly explored, option consists of varying the chain length of the linear component to achieve a variation of properties. Therefore, in the present work, we have taken an aromatic amine-cured DGEBA epoxy and mixed it with PEO with the weight-average molecular mass $M_{w,PEO} \approx 4.0 \times 10^3 \text{ g mol}^{-1}$. A reason for choosing this particular system was also the existence of results for analogous systems containing $M_{w,PEO} \approx 2.0 \times 10^4$ (ref 17) or $\approx 2.0 \times 10^5 \text{ g mol}^{-1}$ (ref 13). Dielectric methods, such as broadband dielectric relaxation spectroscopy (DRS) and thermally stimulated currents (TSCs), were used along with differential scanning calorimetry (DSC), with the aim to acquire information on phase interactions and components' miscibility. Dielectric methods have a well-founded tradition as a tool to evaluate polymer miscibility, since they are sensitive to nanoheterogeneities. In the past, they have been used to verify the existence of a single glass-transition signal (i.e., the common criterion for miscibility) in several fully or semi-IPNs (e.g., polycyanurate-*i*-polyurethane¹⁸) or of multiple segmental relaxation signals in low to moderately cross-linked, phase-separated systems.^{19–21} Dielectric analysis techniques are apparently sensitive to subtle perturbations in the nanoscale relaxation dynamics of the constituting phases induced by their mixing at various ratios.^{22,23} They have been also used to monitor phase separation, gelation, and vitrification processes during cure²⁴ or to study relaxation dynamics in thermosetting systems,^{23,25–30} providing sensitive information regarding the change of the molecular environment of the dielectrically active structural units and of ionic species, in the course of network formation.³⁰ Since segmental relaxation modes determine mobility of space charges, dielectric investigation of systems such as the present one, with effects of varying molecular weight explored, can lead to nanocomposite systems with potential applications as fast ion conductors.^{31,32}

II. Experimental

II. A. Materials. The epoxy resin used in this study and earlier publications^{17,33,34} was DGEBA (EPON resin 828; Shell Chemicals Corporation, U.S.A.) with degree of oligomerization $n \approx 0.1$. The number-average molecular mass is $M_{n(ER)} = 360 \text{ g mol}^{-1}$, with the epoxide equivalent mass near 185 g. PEO (Sigma Chemical Co., USA) with molecular weight $M_w \approx 4.0 \times 10^3 \text{ g mol}^{-1}$ was used without further purification. We employed a common aromatic amine, 4,4'-diaminodiphenylmethane (DDM, chemical grade, $\bar{M}_{n(DDM)} = 198.26 \text{ g mol}^{-1}$) from Aldrich Chemical Inc. (USA) in granular form as the curing agent.

Acetone solutions of the curing agent were mixed at 90 °C (just above curing agent melting point $T_m = 87 \text{ °C}$) with acetone solutions containing DGEBA and predetermined quantities of PEO. The amount of hardener relative to DGEBA was 28 phr (parts per 100), which results in the stoichiometric amino hydrogen/epoxy ratio $[r] = 1$. The parameter $[r]$ is related to the degree of crosslinking; namely,

$$[r] = \frac{4m_{\text{DDM}}/\bar{M}_{n(\text{DDM})}}{2m_{\text{ER}}/\bar{M}_{n(\text{ER})}} \quad (1)$$

where m_{ER} and m_{DDM} are the initial weights of amine and epoxy resin prepolymer in the mixture, respectively. Curing of the well-mixed ternary DGEBA + PEO + DDM blends was performed at 90 °C for 4 h, followed by postcuring at 120 °C for 2 h. Blend compositions will be expressed either in wt % of each

component or in weight fractions; for example, 10/90 ER + PEO means 10 wt % of DGEBA + DDM and 90 wt % PEO. All samples were vacuum-dried at room temperature for at least 3 days and stored in a P_2O_5 desiccator between measurements. For the hydration measurements, each sample was left, until saturation, successively in desiccators with controlled relative humidity environments ranging from 11% to 98%. Once their weight was stabilized, the percentage of absorbed water was calculated as hydration (%) = $[(m_{\text{hydr}} - m_{\text{dry}})/m_{\text{dry}}] \times 100$.

II. B. Techniques. *Broadband Dielectric Relaxation Spectroscopy (DRS).* The complex dielectric permittivity data are represented as $\epsilon^*(f) = \epsilon'(f) - i\epsilon''(f)$. Here, $\epsilon'(f)$ is the real part of the permittivity, $j^2 = -1$, $\epsilon''(f)$ is the dielectric loss, and f is the linear frequency. The values featured in the above function can be analyzed on the basis of a superposition of several terms corresponding to the empirical asymmetric Havriliak–Negami function³⁵ and dc conductivity effects. Thus, one writes

$$\epsilon^*(f) = \epsilon_\infty + \sum_i \frac{\Delta\epsilon_i}{\left[1 + \left(\frac{f}{f_{0,i}}\right)^{1-\alpha_i}\right]^{\beta_i}} - j \frac{\sigma_{\text{dc}}}{\epsilon_0(2\pi f)^s} \quad (2)$$

where σ_{dc} is the dc conductivity of the material, $0 < s \leq 1$ ($s = 1$ for ohmic conductivity), ϵ_0 is the permittivity of free space, and ϵ_∞ is the permittivity at radiowave frequencies. In the framework of the Havriliak–Negami model, the temperature-dependent parameters of the i th relaxation mode are the mean relaxation frequency ($f_{0,i}$); the relaxation strength, $\Delta\epsilon_i$; and the width, α_i , and asymmetry, β_i , of the relaxation in relation to a single-relaxation-time (Debye) process ($\alpha = 1 - \beta = 0$).

Subglassy processes usually exhibit thermally activated relaxation frequencies, represented by an Arrhenius-type equation,

$$f_{\text{max}}(T) = C \exp\left(-\frac{E}{k_\beta T}\right) \quad (3)$$

where C is a mechanism-specific constant, and k_β is the Boltzmann constant. The apparent activation energy barrier, E , obtained from the slope of the $\log(f_{\text{max}})$ versus $1/T$ plot (Arrhenius diagram), depends on both the internal rotation barriers (intramolecular contributions) and the environment of the relaxing unit (intermolecular components). For segmental relaxations, the Vogel–Tammann–Fulcher–Hesse (VTFH) relation³⁶

$$f_{\text{max}}(T) = A \exp\left(-\frac{B}{T - T_V}\right) \quad (4)$$

provides usually an accurate description of the data. A and B are constants, and T_V is the so-called ideal glass transition or Vogel temperature; below T_V , all molecular motions are frozen. The relaxation frequency (f_{max}) of a mechanism at the temperature of the DRS scan is obtained from the Havriliak–Negami parameter, f_0 , using the relation³⁰

$$f_{\text{max}} = f_0 \left\{ \frac{\sin\left[\frac{\pi}{2} \frac{1-\alpha}{\beta+1}\right]}{\sin\left[\frac{\pi}{2} \frac{(1-\alpha)\beta}{\beta+1}\right]} \right\}^{\frac{1}{1-\alpha}} \quad (5)$$

For DRS measurements, disk-like specimens were sandwiched between brass electrodes, and ϵ^* was determined as a function of the frequency (10^{-2} – 10^6 Hz) at selected temperatures between -140 and 150 °C (controlled to better than ± 0.1

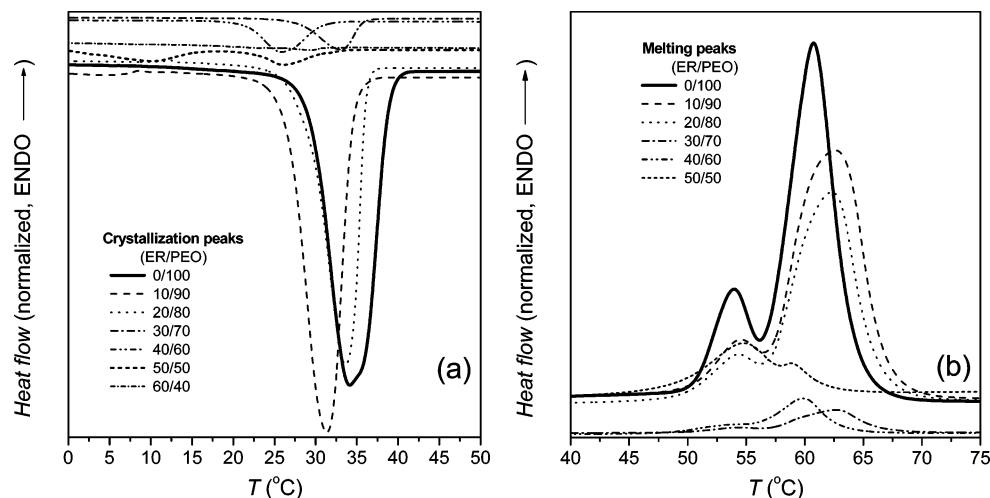


Figure 1. Crystallization (a) and melting (b) peaks recorded for cured DGEBA-*i*-PEO ($M_w = 4000 \text{ g mol}^{-1}$) semi-IPNs. Crystallization peaks were recorded during the second cooling scans, and the melting peaks, during the second heating scans; performed at a rate of $20 \text{ }^\circ\text{C/min}$.

K). A Novocontrol Alpha Analyzer was used in combination with the Novocontrol Quatro Cryosystem.

Thermally Stimulated Currents (TSC). Thermally stimulated currents are a particularly attractive technique based on the measurement of the thermally activated release of stored polarization. Typically, the experiment consists of polarizing a sample at some sufficiently high-temperature, T_p , by applying a static electric field, E_p , for a sufficient period of time, t_p . When sample temperature is lowered to T_0 with the electric field applied and then shorted at T_0 , the nonequilibrium state of the system is frozen-in. During the successive heating, at a constant heating rate $b = dT/dt$, the recovery of the system is monitored by measuring the depolarization current density ($J(T)$). The $J(T)$ thermogram corresponds to a $\epsilon''(T)$ plot at the (low) equivalent frequency of $\sim 10^{-2} - 10^{-4} \text{ Hz}$.³⁷ The method allows for a quick characterization of the overall dielectric response of the material under investigation with high sensitivity and high peak resolving power while offering techniques to analyze experimentally complex relaxation mechanisms into approximately single responses.³⁷

The TSC scans were performed in vacuum ($10^{-2} - 10^{-4} \text{ Pa}$), usually in the range -243 to $+77 \text{ }^\circ\text{C}$ (or to $180 \text{ }^\circ\text{C}$ for blends with $w_{\text{PEO}} \leq 20 \text{ wt } \%$), $E_p \approx 2.0 \times 10^6 \text{ V/m}$, $t_p = 5 \text{ min}$, and $b = 5 \text{ }^\circ\text{C/min}$. Samples of typical dimensions ($5 \times 5 \times 1 \text{ mm}^3$) were used. In each case, T_p was kept below the melting point of the crystalline component. In order to facilitate comparisons between different samples, the TSC spectra are given in transient conductivity units $\sigma(T) = J(T)/E_p$. The amorphous-phase glass transition temperature, T_g , has been defined as that of the maximum current for the α -relaxation peak, T_α .

Differential Scanning Calorimetry (DSC). A Perkin-Elmer Pyris 6 differential scanning calorimeter under a dry nitrogen atmosphere was used (N_2 flow of 20 mL min^{-1}), calibrated with an indium standard. Samples weighting $\approx 5 \text{ mg}$ were rapidly cooled from room temperature to $-120 \text{ }^\circ\text{C}$ and subsequently heated to $110 \text{ }^\circ\text{C}$ and held there for 5 min to eliminate the thermal history. This was followed by a second quenching to $-120 \text{ }^\circ\text{C}$. Finally, the samples were reheated to 200 or $250 \text{ }^\circ\text{C}$ (second scan at a heating rate of $20 \text{ }^\circ\text{C min}^{-1}$). Glass transition temperatures were estimated as the midpoint of the heat capacity change. The apparent melting enthalpy, $H_{m,\text{blend}}$, and melting temperatures, T_m , were determined from the DSC endothermic peaks on the second heating run on the basis of the area and the maximum of the endothermic peaks, respectively. Crystal-

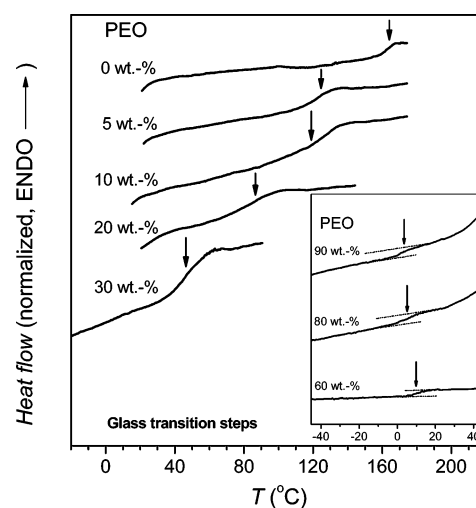


Figure 2. DSC results for selected cured DGEBA-*i*-PEO systems. The glass transition temperatures are indicated by arrows.

lization temperatures, T_c , refer to the principal maximum of the exothermic peaks recorded in the second cooling step.

III. Thermal Characteristics of the ER-*i*-PEO Networks

As a result of curing, the initial mixture undergoes a series of structural changes, for example, growth of chains, branching of chains, and gelation, which convert the initial ternary system into a binary system, ER + PEO. Networks with less than $40 \text{ wt } \%$ PEO were transparent; the remaining ones, opaque. Scanning electron microscopy (SEM) micrographs of selected networks (*not* shown here for brevity) revealed a homogeneous morphology for blends with $w_{\text{PEO}} \leq 40 \text{ wt } \%$ and two phases at higher concentrations. We apparently have an amorphous network—namely, branched epoxy chains mixed with amorphous PEO chains—between PEO lamellae. The creation of polymer chains in the form of crystallites (spherulites^{2,13}) is evidenced by the presence of exothermic crystallization peaks (Figure 1a) and multiple, well-separated, endothermic melting peaks (Figure 1b) in samples with PEO weight fractions $w_{\text{PEO}} > 40 \text{ wt } \%$. The low-temperature component of the complex peaks seen in Figure 1 ($50 - 56 \text{ }^\circ\text{C}$) is assumed to arise from homogeneous nucleation, whereas the higher ($58 - 63 \text{ }^\circ\text{C}$), from heterogeneous nucleation. The absence of cold-crystallization

TABLE 1: Thermophysical Characteristics of the Blends: T_g , T_m , Heat Capacity Change at Glass Transition ΔC_p , T_c , and Percentages of Crystallinity of the PEO Component in the Blends X_c and of the Cured ER + PEO Blends $X_{c,blend}$ ^a

w_{PEO} (wt %)	T_g (°C)	ΔC_p (J/g·K)	T_m (°C)	$H_{m,blend}$ (J/g)	T_c (°C)	X_c (%)	$X_{c,blend}$ (%)	w'_{PEO} (wt %)
0	162	0.267						
5	124	0.265						
10	116.6	0.365						
20	84.7	0.318						
30	45.8	0.349						
40				4.5	23.8	5	2	38
50	-8.7	0.129	54.5	42.5	28.2	33	21	36
60	10.1	0.215	58.7	79.4	25.7	64	39	34
70			61.0	96.6	33.1	67	47	43
80	5.7	0.100	61.3	121.6	33.8	74	59	51
90	3.5	0.235	62.1	155.0	31.3	84	75	60
100	-40 ^b		62.0	167.7	34.2	81		

^a The weight percentage of PEO in the amorphous phase (w'_{PEO}) is also included. ^b The glass transition step observed in this sample was nearly indiscernible, and thus, a literature value is used (Brandrup, J.; Immergut, E. H. *Polymer Handbook*; 3rd ed.; Wiley: New York, 1989.).

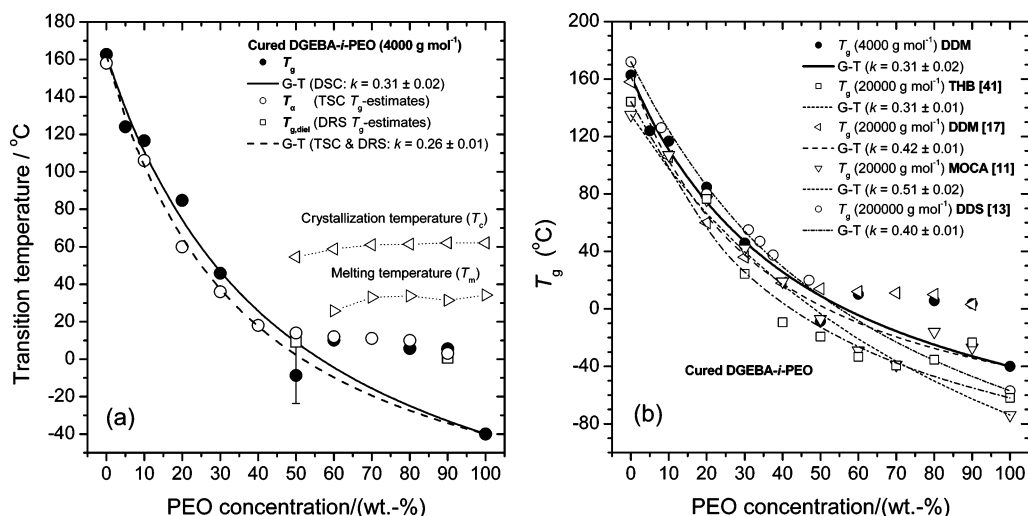


Figure 3. (a) Plots of transition temperatures as function of blend composition for the thermosetting networks prepared with PEO (4.0×10^3 g mol⁻¹). Data-fitting lines based on the Gordon–Taylor equation are shown. (b) Comparison of the compositional variation of calorimetric T_g 's and the k parameter estimates for several networks.

transitions during the second heating run indicates that crystallization was rapid and occurred to completion during the quenching.

DSC curves shown in Figure 2 exhibit relatively weak glass transition regions for most compositions. The thermophysical characteristics so obtained are listed in Table 1. The degree of crystallinity (X_c and $X_{c,blend}$) was calculated by dividing, respectively, $H_{m,PEO}$ and $H_{m,blend}$ —the apparent melting enthalpies per gram of blend and of PEO present in the blend—by $H_m^0 = 205$ J/g (for perfectly crystallized PEO). We see in Table 1 that the crystallinity of the blends decreases with increasing concentration of the noncrystallizable epoxy component (ER), as expected. Formation of the cross-linked epoxy network influences the PEO crystallization. In our case, significant crystalline PEO nanodomains, that is, $X_{c,blend} > 10\%$, are formed between 40 and 50 wt % PEO instead of 60 wt % PEO, as in ref 17. We conclude from this comparison that in our case, shorter PEO chains organize themselves more easily into crystalline domains.

Observation of single calorimetric glass transition peaks (or equivalently of dielectric and mechanical segmental relaxations) between the constituent values for the amorphous components is regarded as clear manifestation of phase miscibility in binary cured thermoset + polymer systems.^{12–16} Figure 3a shows the glass transition temperatures, T_g , the melting temperatures, T_m , and crystallization temperatures, T_c , as a function of composition. Deviations of the T_g curve on the right-hand side from a

simple concave shape will be a subject of a separate publication. For the needs of the present work and consonant with most of the DSC studies of similar networks, we have used the empirical Gordon–Taylor (G–T) equation.³⁸

$$T_g^{blend} = \frac{w_{PEO}T_g^{PEO} + kw_{ER}T_g^{ER}}{w_{PEO} + kw_{ER}} \quad (6)$$

Equation 6 represents the mixing contribution derived from the additive rule of entropy, of the volume of the blends, or both. The adjusting parameter, k , has been used as a semiquantitative measure of miscibility and strength of the intermolecular interactions among the components of polymer blends: higher k indicates an increased amount or strength of intermolecular hydrogen-bonding³⁹ and of other secondary interaction forces. The negative deviation of the compositional dependences of calorimetric and dielectric T_g estimates (T_α from TSC and $T_{g,die}$ from DRS; see the following section for details) from linear mixing for PEO loadings below 50 wt % can be well-described by the G–T equation with very low k values ($k_{die} = 0.26$, $k_{DSC} = 0.31$). This is usually considered a consequence of a decreased enthalpy contribution, which in turn indicates weakened intermolecular-specific phase interactions in the cross-linked structures.^{12,37,38} The above estimates are clearly below those recently reported for networks prepared with the same curing agent and PEO of higher molecular weight (2.0×10^4 g mol⁻¹), $k_{TSC} = 0.32$, $k_{DSC} = 0.42$ (Figure 3b; ref 17). A comparison of the

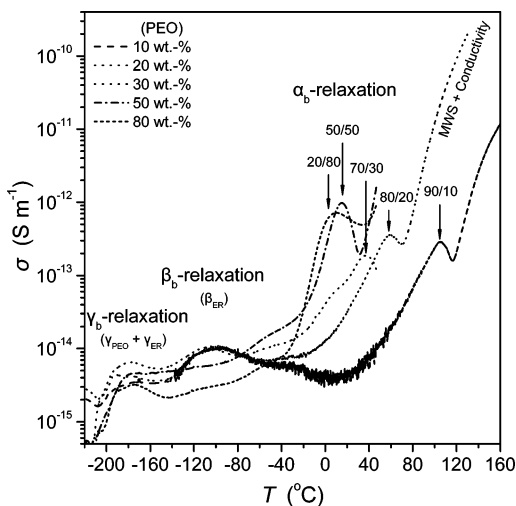


Figure 4. Transient conductivity $\sigma(T)$ spectra of selected ER-*i*-PEO networks.

T_g -vs- w_{PEO} dependences included in Figure 3b reveals a weakening of the strength and of the extent of the phase interactions with a decrease in the molecular weight of the PEO. Although no general trends can be determined from the available literature data, it is clear that both the nature and the amount of the curing agent have a sound influence on the magnitude of the k parameter.

Strong positive deviation of the experimental T_g 's from the fitting curves appears above ~ 40 wt % PEO. This departure is related to the compositional enrichment of the amorphous region, created by crystallization of PEO (i.e., increase of the ER concentration in the residual amorphous PEO phase). Moreover, an increase in the glass transition temperature is expected due to the stiffening of the amorphous phase by reinforcement from PEO spherulites.⁷ This agrees with several calorimetric results^{2,8,15} and appears independent of the type and content of the hardener. It is clear, though, from the data included in Figure 3b that the exact threshold is highly dependent on the nature of the curing agent, spanning the range between ~ 50 ¹⁷ and 80^{11,41} wt % PEO. Direct comparison of our data with the data for $M_{w(PEO)} \approx 2.0 \times 10^4$ g mol⁻¹ suggests that the lowering of the molecular weight enhances the ability of PEO to diffuse and crystallize within the amorphous network. The melting temperature of the crystalline component in the blends slightly decreases with an increase in w_{ER} , a behavior characteristic of miscible blends. It should be noted, however, that in the present system, the T_m depression appears neither strong nor consistent so as to provide an unambiguous criterion for phase miscibility.

IV. Relaxation Dynamics of the ER-*i*-PEO Networks

IV. A. Thermally Stimulated Current Analysis. We show in Figure 4 transient conductivity $\sigma(T)$ signals in thick films of selected vacuum-dried ER-*i*-PEO samples. TSC spectra of networks with $w_{PEO} > 50$ wt % were recorded with the MISIM electrode configuration (M = copper electrode electrolytically covered by chromium, I = thin insulating Teflon foil, S = sample) to separate the relaxation response from intense high- T dc conductivity signals. In the TSC spectra, the glass transition region is traditionally called α_b relaxation. For aromatic amine-cured DGEBA, the glass transition signal peaks at $T_\alpha = 158$ °C, reasonably close to the calorimetric $T_g \approx 162$ °C. The peak shifts steadily to lower temperatures as w_{PEO} increases from 0 to 50 wt %, in agreement with the DSC data (Figure 3a). The behavior changes when the linear polyether starts to phase-

separate and form crystalline nanodomains dispersed in an amorphous environment. The two techniques provide mutually complementary results. To give one more example, for $w_{PEO} = 90$ wt %, the α_b relaxation maximizes at $T_\alpha = +3$ °C, whereas the midpoint of the heat capacity change gives $T_g = +5.5$ °C.

A secondary signal (β_b) is present for all network compositions studied ($0 \leq w_{PEO} \leq 90$ wt %). It reflects the onset of mobility of short segments of the thermosetting component (i.e., the so-called β_{ER} relaxation). For neat epoxy resin, this occurs around -108 °C, in agreement with Shin and co-workers.²⁵ Several DGEBA systems with other curing agents show this TSC signal in the same temperature range; e.g., -100 °C $< \beta_{ER} < -80$ °C for DDS-cured tetraglycidyl-4,4'-diaminodiphenyl methane (TGDDM) and -113 °C $< \beta_{ER} < -73$ °C for triethylenetetramine (TETA)-cured DGEBA.^{27,29} In terms of the amino cross-linked epoxy systems, the β_{ER} relaxation is attributed to the crankshaft motion of the hydroxyether groups (glyceryl segment), which most of them form after the amine-epoxy curing reaction. Earlier TSC and thermally stimulated creep studies of amine-cured epoxy networks revealed that the magnitude of the β_{ER} mode increases with increasing cross-link density.⁴²

Still, below β_b , we have one more complex relaxation process, call it γ_b , between -210 and -120 °C. A part of this signal can be ascribed to a diffuse low- T γ_{ER} mode, a main-chain motion, likely of the glycidyl ether segment. The corresponding TSC signal appears here at temperatures well below -140 °C ($T_{max} \approx -113$ °C,²⁸ -123 °C,^{27,29} -145 °C,²⁵ and -155 °C⁴²). Among others, Mangion and Johari²⁶ observed that the concentration of unreacted epoxy groups decreases, as it should, with increasing cross-linked density, reached at longer curing and postcuring (or aging) programs. In addition, Boye and co-workers⁴² reported a drop of the γ_{ER} TSC band with an increase in $[r]$ from 0.5 to 1 (i.e., increased cross-linking density). In our case, the low dielectric strength of the γ_{ER} mode is consistent with the high cross-linking density obtained for $[r] = 1$. The dielectric γ_b -relaxation mode also incorporates a secondary γ_{PEO} process around -170 °C that is related to thermal depolarization through local twisting movements (crank-shaft or kink motion) in PEO chains in defective regions within crystallites and in noncrystalline regions.⁴³

IV. B. Frequency-Domain Dielectric Analysis. A representative example of the frequency and temperature dependences of dielectric loss factor ϵ'' and the electrical loss, M'' (the imaginary part of the electric modulus),⁴⁴

$$M''(f) = \frac{\epsilon''(f)}{\epsilon'^2(f) + \epsilon''^2(f)} \quad (7)$$

is shown in Figure 5 for a dry ER-*i*-PEO network with $w_{PEO} = 20$ wt %. In agreement with TSC, the main phenomena observed in order of increasing frequency in isothermal plots (or decreasing temperature in isochronal plots) are effects due to macroscopic charge transfer (i.e., the "conductivity relaxation" (CR) mechanism,⁴⁵ with possible contribution from Maxwell-Wagner-Sillars (MWS) polarization effects), cooperative motions of chain segments (α_b), and localized molecular motions responsible for the weaker secondary relaxations (β_b and γ_b).

At low temperatures, the $M''(f)$ spectrum of the network shows the γ_b relaxation at high frequencies with a very small contribution to the overall relaxation response.⁴⁶ Although many TSC spectra reveal a bimodal nature for the γ_b signal, the high-frequency DRS response does not appear to be a superposition of two relaxation mechanisms. Irrespective of the exact network

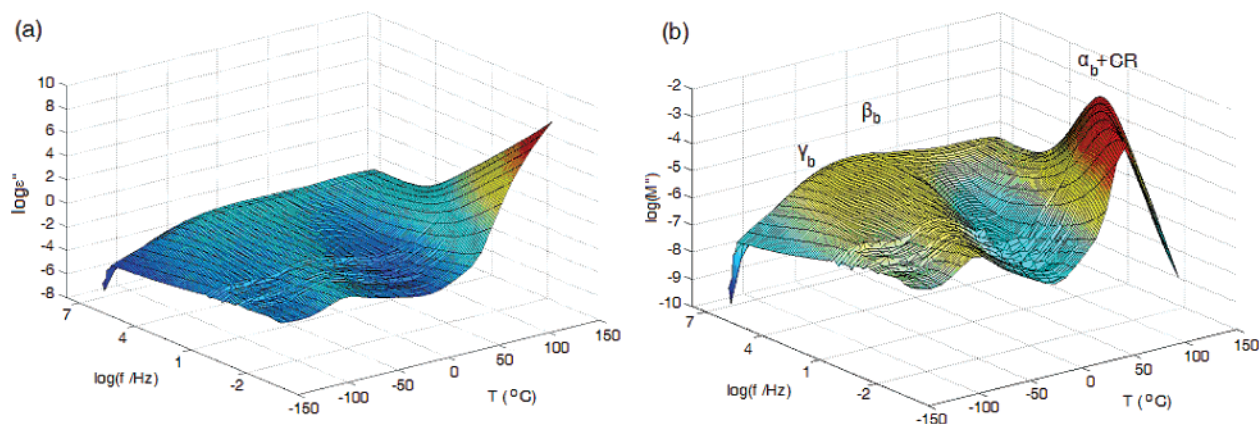


Figure 5. Plot of the temperature and frequency dependencies of the complex parts of the relative dielectric permittivity (ϵ'' ; plot a) and of the electric modulus (M'' , plot b) for the ER/PEO 80/20 network. The main relaxation modes are indicated.

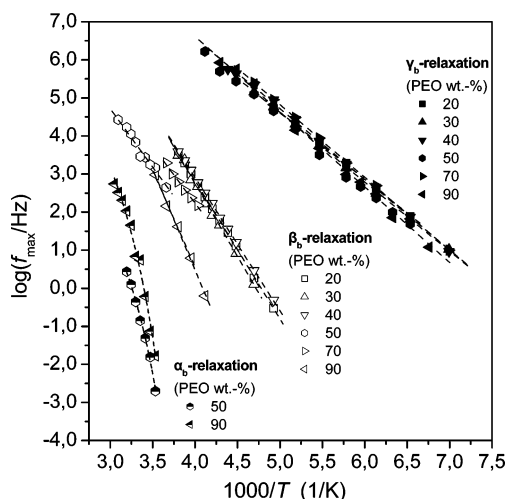


Figure 6. Arrhenius plots for the relaxation mechanisms isolated in selected ER-*i*-PEO networks ($w_{\text{PEO}} = 20, 30, 40, 50, 70,$ or 90 wt %). The lines are fits of the experimental data to the Arrhenius eq 3 or the VTFH eq 4.

composition, both secondary relaxations (γ_b and β_b) are broad, with a half-width of the M'' signal much greater than that of the Debye peak (1.14 decades), confirming that the mechanisms are characterized by a broad distribution of relaxation times. This result illustrates the heterogeneous structure of the material.

The analysis of the isothermal DRS spectra was performed with use of the semiempirical Havriliak–Negami equation. The Arrhenius-type relation (eq 3) has been used to fit subglassy relaxations, whereas the VTFH relation (eq 4) was used for the segmental relaxation mode (Figure 6). The strong overlapping of the CR, MWS, and α -relaxation signals made it impossible to monitor by means of DRS changes in the segmental relaxation dynamics for a number of networks. For two-blend compositions, it has been possible to calculate the dielectric glass transition temperature ($T_{g,\text{diel}}$), defined by the convention $\tau(T_{g,\text{diel}}) = 100$ s so that it corresponds to the temperature at which the loss factor band peaks at $f_{\text{max}} = 1.6 \times 10^{-3}$ Hz. Using the data shown in Figure 6, we obtained values of $T_{g,\text{diel}}$ in very good agreement with the TSC- and DSC-based glass transition temperature estimates (see Figure 3a).

The temperature dependence of the dielectric strengths of the β_b and γ_b relaxation signals is shown in Figure 7. $\Delta\epsilon_{\gamma(\text{blend})}$ clearly decreases with decreasing ER concentration; apparently, the main contribution to this mechanism arises from the γ_{ER} relaxation mode. The relaxation frequencies of the γ_b -relaxation mechanism (Figure 6) and the corresponding activation energy

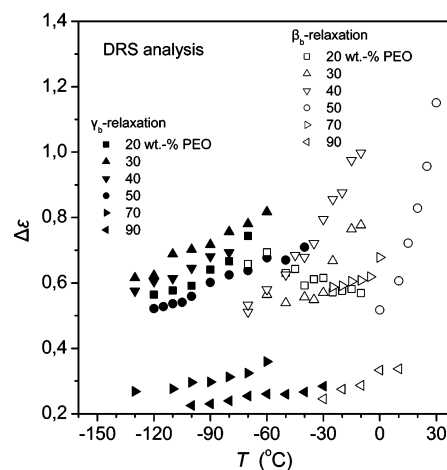


Figure 7. Temperature dependence of the dielectric strength $\Delta\epsilon_\beta$ and $\Delta\epsilon_\gamma$ of the secondary mechanisms isolated in selected ER-*i*-PEO networks.

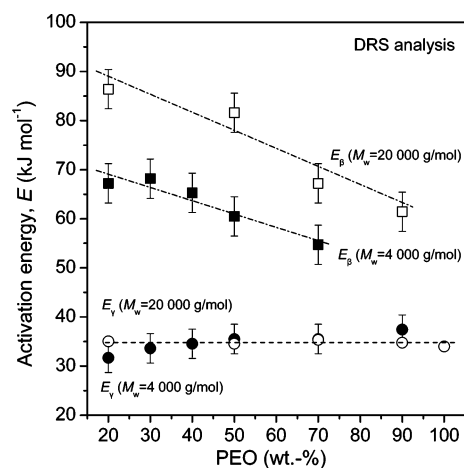


Figure 8. Compositional dependence of the apparent activation energies of the secondary modes isolated in selected ER-*i*-PEO networks. The data for $M_{w(\text{PEO})} \approx 2.0 \times 10^4$ g mol $^{-1}$ are taken from ref 17.

barriers ($E_{\gamma(\text{blend})} = 35 \pm 3$ kJ/mol; Figure 8) are nearly independent of the network composition. The $E_{\gamma(\text{blend})}$ values are in the range from 20 to 50 kJ/mol, typical for local relaxation mechanisms in polymers.⁴⁷ The activation energy barriers for the β_b -relaxation mechanism ($E_{\beta(\text{blend})}$) exhibit a gradual decrease with increasing PEO concentration (Figure 8). The compositional variation of $\Delta\epsilon_{\beta(\text{blend})}$ seems to be rather irregular (Figure 9a). Nevertheless, the plasticizing effect of the addition of the

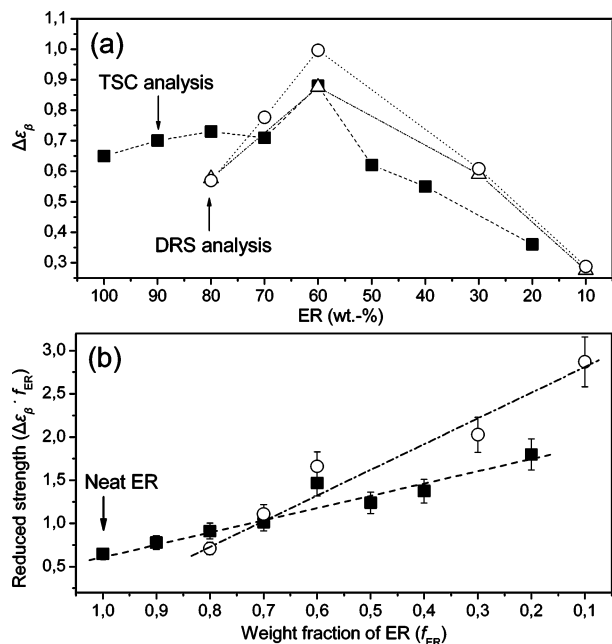


Figure 9. Dielectric strengths of the secondary β_b -relaxation. (a) Compositional dependence of $\Delta\epsilon_\beta$ for the mechanism isolated in selected ER-*i*-PEO networks (20, 30, 40, 50, 70, and 90 wt % PEO). (b) Plot of the reduced strength of the β_b -relaxation signals ($\Delta\epsilon_\beta \times f_{ER}$) as a function of the weight fraction of ER in the network (f_{ER}). (■, TSC and ○, DRS data of our $M_{w(PEO)} \approx 4.0 \times 10^3$ g mol⁻¹; △, DRS data from ref 17 for $M_{w(PEO)} \approx 2.0 \times 10^4$ g mol⁻¹).

linear polyether chains on the β -relaxation signal of the epoxy resin becomes evident in the plot of the reduced strengths, $\Delta\epsilon_{\beta(\text{reduced})} = \Delta\epsilon_\beta \times f_{ER}$, as a function of the actual weight fraction of ER in the network (f_{ER}) (Figure 9b). This observation is also in agreement with the clear drop of the apparent activation energy barriers (Figure 8).

Certain characteristics of the mechanisms related to macroscopic mobility (space-charge motions and the segmental relaxation) show strong dependence on the equilibrium hydration level, h , of the semi-IPNs. The high-frequency shift of the glass-transition signal (Figure 10a) with an increase in h , attained for relative humidity environments increasing from 0 to 75%, reflects a plasticization caused by occlusion of water molecules. By increasing the content of the polyetheric modifier, the

network develops higher permeability to water molecules. In turn, this facilitates also the local motion of short chain segments (Figure 10b). The strong departure from linearity of the dc conductivity (σ_{dc}) and the water uptake, h , in % vs relative humidity (RH, also in %) reflects structural changes in the polymer network caused by PEO (Figure 11). The parallel behavior of these two distinctly different parameters reveals the role of migrating protons and their impact on the conductivity and water sorption mechanisms.

V. Concluding Remarks

We have analyzed the strength of intra- and intermolecular interactions, the degree of mixing, and other characteristics of the cure products. The relaxation characteristics of secondary modes related to local chain mobility show insensitiveness to $M_{w(PEO)}$. The β -relaxation of the thermosetting component, in particular, is plasticized by the addition of poly(ethylene oxide), irrespective of the length of the linear chain (Figures 8 and 9). This provides a strong indication of changes in the molecular environment of the relaxing glyceryl segments, further manifested by the lowering in the strength of the intermolecular interactions. The negative dependence of the T_g 's is also in accordance with the above finding. The estimates for the parameter k of the Gordon–Taylor equation are in the range 0.26–0.31 (Figure 3a), clearly lower than those previously reported for similar networks incorporating longer PEO chains and chemically dissimilar curing agents ($0.3 \leq k \leq 0.5$; Figure 3b).

The basic interaction force between the constituent chain segments appears to be hydrogen bonding between group pairs, such as the hydroxyl (–OH) of epoxy and the ether group (–O–) of PEO, which act antagonistically to the self-association of hydroxyls in pure ER. As the hydrogen bond is a directional, attractive interaction between electron-deficient hydrogen and a region of high electron density, its strength is directly related to all the elements affecting the acidity of the proton donor, the basicity of the proton acceptor, the accessibility of the donor and acceptor, and the chemical and stereo structures of the donors and acceptors. In the present case, the formation of the cross-linked network enhances steric shielding (the “screening effect”) and decreases the accessibility of functional groups, resulting in a reduction of the specific interactions between PEO and ER chains.^{8,13} The reduction of the k values may be in part

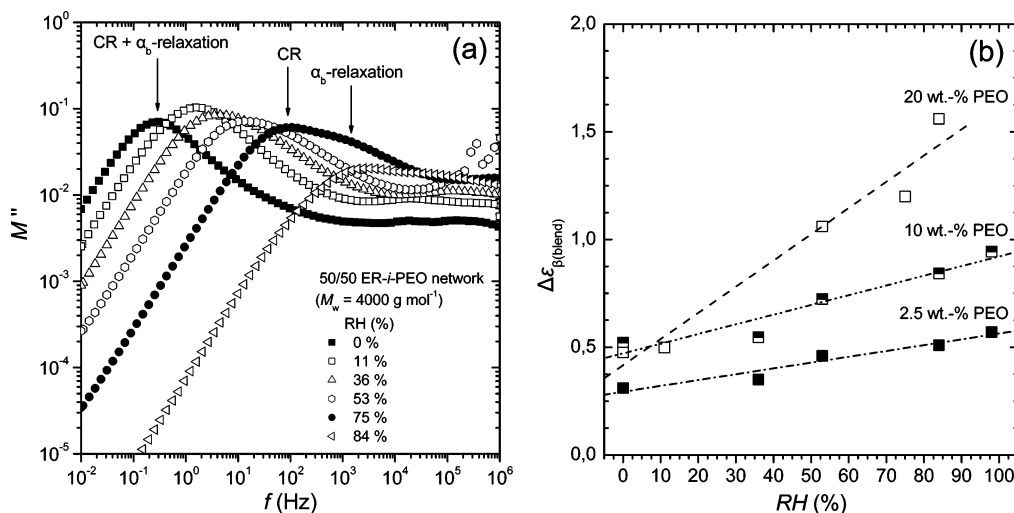


Figure 10. (a) Modification of the $M''(f)$ spectrum at room temperature of the 50/50 ER + PEO blend as result of (equilibrium) water absorption attained at various levels of relative humidity (RH %). (b) Water-induced plasticization of the β_b -relaxation mode in the blends (room-temperature data) is clearly demonstrated by the amplification of the relaxation strength with increase of the hydration level (at higher RHs).

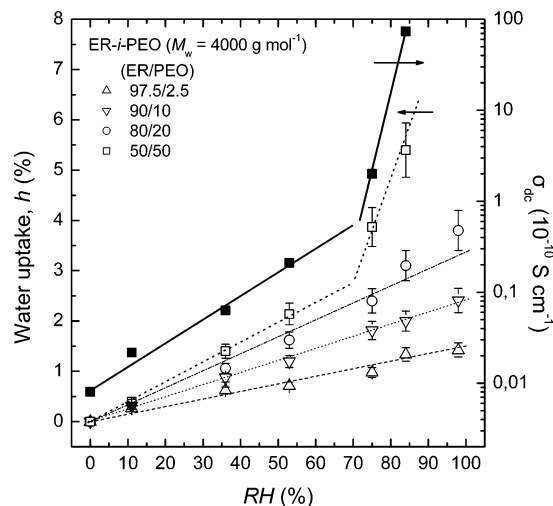


Figure 11. Plot of the dc conductivity (σ_{dc}) and the water uptake (h %) as function of RH (%) (room-temperature data). The error shown for the water uptake percentages accounts for $\pm 10\%$ of the experimental values. The dashed/dotted lines describe the variation of the water uptake experimental points, and the solid line is for the conductivity estimates (for the 50/50 ER/PEO sample).

related to the improved penetration of the resin network by the shorter PEO chains. This should enhance the number of weak intercomponent hydrogen-bonding interactions ($[ER]-OH \cdots O < [PEO]$ bonds) in the ER-*i*-PEO networks, against the population of the antagonistic, strong self-association of the hydroxyl groups ($-OH \cdots OH-$ linkages) between neat resin chains. The above deduction is consistent with the observation that the use of low-molecular-weight PEO activates both homogeneous and heterogeneous crystallization centers (Figure 1b). That is, crystallization occurs in different molecular environments. We recall that substantial crystalline PEO nanodomains form at $w_{PEO} \sim 45$ wt % for $M_{w(PEO)} \approx 4.0 \times 10^3$ g mol $^{-1}$, as compared to the higher loadings (60–80 wt %) needed when $M_{w(PEO)} \geq 2.0 \times 10^4$ g mol $^{-1}$. This suggests that the decrease in the length of modifier's chains increases their "diffusivity" into the thermosetting network in such a way that facilitates the creation of crystallites at lower PEO loadings. Further studies are required to elucidate this point (comparative SEM studies of blends with different $M_{w(PEO)}$ are now in progress).

An interesting issue in the development of novel network compositions is the relative impact of different thermodynamic and chemical factors on achieving components miscibility. An extensive network of strong hydrogen-bonding interactions is believed essential for miscibility.⁴⁸ However, there are cases in which ER-*i*-PEO networks may be either miscible (e.g., using DDS as crosslinker) or phase-separated (e.g., with DETA), in spite of the high strength of the hydrogen bonds confirmed by infrared spectroscopy.¹³ Homogeneous structures have been reported even for blends cured with aromatic anhydrides (e.g., PMDA), for which structural similarity with the cure components is present but hydrogen bonding is not expected.¹³ Furthermore, the structurally "incompatible" aliphatic curing agents fall short of producing homogeneous ER-*i*-PEO networks. The above observations strengthen the following: the presence of hydrogen-bonding sites between specific functional groups is neither a sufficient nor a necessary condition for phase homogeneity. The present results (i.e., the weakening of the strength of the intermolecular interactions) support the idea that structural similarity of the components (resin, curing agent, and polyether) and the number of interassociated hydrogen bonds

(rather than the strength of the bond itself) regulate the miscibility or compatibility of the particular DDM-cured ER-*i*-PEO networks.

Acknowledgment. The authors express their gratitude to Dorota Pietkiewicz of LAPOM for providing the materials for our study. The present research has been funded by E.P.E.A.K. 2 (Operational Programme for Education and Initial Vocational Training), Athens, in the frame of PYTHAGORAS (Project 70/3/7362) and also by the Robert A. Welch Foundation, Houston (Grant B-1203). Gay Woods and Alex Potemkin of the University of North Texas participated in the literature search.

References and Notes

- Mark, J. E.; Erman, B. *Elastomers and Rubber-like Elasticity. In Performance of Plastics*; Brostow, W., Ed.; Hanser: Munich, Cincinnati, 2000; Chapter 17.
- Pearce, E. M.; Wright, C. E.; Bordoloi, B. K. *J. Mater. Ed.* **1980**, *2*, 931.
- Mark, J. E. *J. Mater. Ed.* **1982**, *4*, 733.
- Csernica, J. J. *J. Mater. Ed.* **1993**, *15*, 249.
- Bilyeu, B.; Brostow, W.; Menard, K. P. *J. Mater. Ed.* **2001**, *23*, 189.
- Guo, Q.; Peng, X.; Wang, Z. *Polymer* **1991**, *32*, 53.
- Venderbosch, R. W.; Meijier, H. E. H.; Lemstra, P. J. *Polymer* **1995**, *36*, 2903.
- Naffakh, M.; Dumon, M.; Gerard, J. F. *Compos. Sci. Technol.* **2006**, *66*, 1376.
- Giannotti, M. I.; Mondragon, I.; Galante, M. J.; Oyanguren, P. A. *J. Polym. Sci. Phys.* **2004**, *42*, 3964.
- Li, L.; Liu, M. J.; Li, S. J. *Polymer* **2004**, *45*, 2837.
- Lü, H.; Zheng, S. *Polymer* **2003**, *44*, 4689.
- Hu, L.; Lü, H.; Zheng, S. *J. Polym. Sci. Phys.* **2004**, *42*, 2567.
- Iriarte, M.; Espi, E.; Etxeberria, A.; Valero, M.; Fernandez-Berridi, M. J.; Iruin, J. J. *Macromolecules* **1991**, *24*, 5546.
- Robeson, L. M.; Hale, W. F.; Merriam, C. N. *Macromolecules* **1981**, *14*, 1644.
- Yin, M.; Zheng, S. *Macromol. Chem. Phys.* **2005**, *206*, 929.
- Zheng, S.; Zhang, N.; Luo, X.; Ma, D. *Polymer* **1995**, *36*, 3609.
- Horng, T. J.; Woo, E. M. *Polymer* **1998**, *39*, 4115.
- Horng, T. J.; Woo, E. M. *Angew. Makromol. Chem.* **1998**, *260*, 31.
- Guo, Q.; Harrats, C.; Groeninckx, G.; Koch, M. H. J. *Polymer* **2001**, *42*, 4127.
- Luo, X.; Zheng, S.; Zhang, N.; Ma, D. *Polymer* **1994**, *35*, 2619.
- Kalogeras, I. M.; Vassilikou-Dova, A.; Christakis, I.; Pietkiewicz, D.; Brostow, W. *Macromol. Chem. Phys.* **2006**, *207*, 879.
- Kim, S. J.; Park, S. J.; Kim, I. Y.; Lee, Y. H.; Kim, S. I. *J. Appl. Polym. Sci.* **2002**, *86*, 1844.
- Shin, M. S.; Kim, S. J.; Park, S. J.; Lee, Y. H.; Kim, S. I. *J. Appl. Polym. Sci.* **2002**, *86*, 498.
- Karabanova, L. V.; Boiteux, G.; Gain, O.; Seytre, G.; Sergeeva, L. M.; Lutsyk, E. D.; Bodarenko, P. A. *J. Appl. Polym. Sci.* **2003**, *90*, 1191.
- Sanchez, M. S.; Ferrer, G. G.; Cabanilles, C. T.; Duenas, J. M. M.; Pradas, M. M.; Ribelles, J. L. G. *Polymer* **2001**, *42*, 10071.
- Corezzi, S.; Beiner, M.; Huth, H.; Schröter, K.; Capaccioli, S.; Casalini, R.; Fioretto, D.; Donth, E. E. *J. Chem. Phys.* **2002**, *117*, 2435.
- Beiner, M.; Ngai, K. L. *Macromolecules* **2005**, *38*, 7033.
- Alig, I.; Jenninger, W. *J. Polym. Sci. Phys.* **1998**, *38*, 2461.
- Shin, S. M.; Shin, D. K.; Lee, D. C. *Polym. Bull.* **1998**, *40*, 599.
- Mangion, M. B. M.; Johari, G. P. *J. Polym. Sci. Phys.* **1991**, *29*, 437.
- Su, W.-F. A.; Carr, S. H.; Brittain, J. O. *J. Polym. Sci. Phys.* **1980**, *25*, 1355.
- Lee, J. Y.; Song, Y. W.; Kim, S. W.; Lee, H. K. *Mater. Chem. Phys.* **2003**, *77*, 455.
- Maggana, C.; Pissis, P. *J. Macromol. Sci.-Phys. B* **1997**, *36*, 749.
- Vassilikou-Dova, A.; Kalogeras, I. M. *Dielectric Analysis. In Thermal Analysis of Polymers: Fundamentals and Applications*; Prime, R. B.; Menczel, J., Eds.; Wiley: New York, in press; Chapter 6.
- Chu, P. P.; Reddy, M. J.; Tsai, J. J. *J. Polym. Sci. Phys.* **2004**, *42*, 3866.
- Rocco, A. M.; Fonseca, C. P.; Loureiro, F. A. M.; Pereira, R. P. *Solid State Ionics* **2004**, *166*, 115.
- Brostow, W.; Cassidy, P. E.; Hagg, H. E.; Jaklewicz, M.; Montemartini, P. E. *Polymer* **2001**, *42*, 7971.
- Brostow, W.; Bujard, B.; Cassidy, P. E.; Hagg, H. E.; Montemartini, P. E. *Mater. Res. Innovations* **2001**, *6*, 7.
- Havriliak, S., Jr.; Havriliak, S. J. *Dielectric and Mechanical Relaxation in Materials*; Hanser: Munich, 1997; p 14.

- (36) Vogel, H. *Phys. Z.* **1921**, 22, 645. Tammann, G.; Hesse, G. *Z. Anorg. Allg. Chem.* **1926**, 56, 245. Fulcher, G. S. *J. Am. Ceram. Soc.* **1925**, 8, 339.
- (37) Vanderschueren, J.; Gasiot, J. Field-Induced Thermally Stimulated Currents. In *Topics in Applied Physics*; Sessler, G. M., Ed.; Springer: Berlin, 1980.
- (38) Gordon, M.; Taylor, J. S. *J. Appl. Chem.* **1952**, 2, 493.
- (39) Chiu, F. C.; Min, K. S. *Polym. Int.* **2000**, 49, 223.
- (40) Lu, X.; Weiss, R. A. *Macromolecules* **1992**, 25, 3242.
- (41) Zheng, S.; Lü, H.; Chen, C.; Nie, K.; Guo, Q. *Colloid Polym. Sci.* **2003**, 281, 1015.
- (42) Boye, J.; Demont, P.; Lacabanne, C. *J. Polym. Sci. Phys.* **1994**, 32, 1359.
- (43) Ishida, Y.; Matsuo, M.; Takayanagi, M. *J. Polym. Sci. Phys.* **1965**, 3, 321.
- (44) Hodge, I. M.; Ngai, K. L.; Moynihan, C. T. *J. Non-Cryst. Solids* **2005**, 351, 104.
- (45) Jain, H.; Ngai, K. L.; Wright, G. B., Eds. *Relaxation in complex systems*. Naval Research Laboratory: Washington, D.C. 1984; p 221.
- (46) Zong, L.; Zhou, S.; Sun, R.; Kempel, L. C.; Hawley, M. C. *J. Polym. Sci. Phys.* **2004**, 42, 2871.
- (47) Schönhals, A. In *Dielectric Spectroscopy of Polymeric Materials: Fundamentals and Applications*; Runt, J. P., Fitzgerald, J. J., Eds.; American Chemical Society: Washington D.C., 1997; p 107.
- (48) Francis, B.; Thomas, S.; Thomas, S. P.; Ramaswamy, R.; Rao, V. L. *Colloid Polym. Sci.* **2006**, 285, 83.